EPEC recruits a Cdc42-specific GEF, Frabin, to facilitate PAK activation and host cell colonization

Vikash Singh[a], Peter J. Hume[a], Anthony Davidson[a] and Vassilis Koronakis[a*]

[a] Department of Pathology, University of Cambridge, Cambridge, UK

[*] Correspondence:*vk103@cam.ac.uk*

Abstract

Enteropathogenic *Escherichia coli* (EPEC) is an extracellular pathogen that tightly adheres to host cells by forming “actin pedestals” beneath the bacteria, a critical step in pathogenesis. EPEC injects effector proteins that manipulate host cell signalling cascades to trigger pedestal assembly. We have recently shown that one such effector, EspG, hijacks p21-activated kinase (PAK) and sustains its activated state to drive the cytoskeletal changes necessary for attachment of the pathogen to target cells. This EspG subversion of PAK required active Rho family small GTPases in the host cell. Here we show that EPEC itself promotes the activation of Rho GTPases by recruiting Frabin, a host guanine nucleotide exchange factor (GEF) for the Rho GTPase Cdc42. Cells devoid of Frabin showed significantly lower EPEC-induced PAK activation, pedestal formation and bacterial attachment. Frabin recruitment to sites of EPEC attachment was driven by EspG and required localized enrichment of phosphatidylinositol 4,5 bisphosphate (PIP2) and host Arf6. Our findings identify Frabin as a key target for EPEC to ensure the activation status of cellular GTPases required for actin pedestal formation.

Importance

Enteropathogenic Escherichia coli (EPEC) is a leading cause of diarrhea in children, especially in the developing world. EPEC initiates infection by attaching to cells in the host intestine, triggering the formation of actin-rich “pedestal” structures directly beneath the adherent pathogen. These bacteria inject their own receptor into host

cells, which upon binding to a protein on the pathogen surface triggers pedestal formation. Multiple other proteins are also delivered into the cells of the host intestine, which work together to hijack host signaling pathways to drive pedestal production. Here, we show how EPEC hijacks a host protein, Frabin, which creates the conditions in the cell necessary for the pathogen to manipulate a specific pathway that promotes pedestal formation. This provides new insights into this essential early stage in disease caused by EPEC.

Introduction

Enteropathogenic and enterohemorrhagic *E. Coli* (EPEC and EHEC) are bacterial pathogens that are responsible for significant morbidity and mortality globally(1, 2). EPEC causes diarrhoea in children, especially in the developing world(3), while EHEC is associated with outbreaks of acute gastroenteritis and bloody diarrhoea, often linked to contaminated food and sometimes leading to life-threatening complications(4). Following ingestion, EPEC and EHEC tightly adhere to intestinal epithelial cells and cause morphological changes leading to the loss of brush border microvilli, forming characteristic attaching and effacing (A/E) lesions(5). Extensive reorganisation of the host cell cytoskeleton beneath the adherent pathogens leads to the formation of characteristic actin 'pedestals'(6). These structures, which are seemingly crucial for pathogenesis(6), strengthen the attachment of the bacteria to the host epithelium, and also may drive the movement of the adherent pathogen across the epithelial surface, promoting the formation of microcolonies and potentially allowing spread to adjacent cells(7, 8).

Both EPEC and EHEC utilize a type 3 secretion system (T3SS) to deliver a battery of virulence effector proteins into host cells, in order to subvert the cellular signaling networks necessary to drive the cytoskeletal rearrangements underlying pedestal formation(9). We recently reported that one of these effectors, EspG, hijacks host p-21 activated kinase (PAK) to facilitate pedestal formation and bacterial attachment(10). EspG was only able to subvert PAK in the presence of active Rho family small GTPases, which function to both concentrate PAK at the membrane and stimulate PAK activation(10).

Rho GTPases are master regulators of numerous eukaryotic signaling networks(11) and are consequently common targets for subversion by bacterial pathogens(12). For example, several bacteria release toxins which modify GTPases to bring about their permanent activation(13). Other pathogens deliver effectors that mimic host regulators of GTPase signaling, such as guanine nucleotide exchange factors (GEFs; activators)(14) and GTPase activating proteins (GAPs; inactivators)(15). EPEC and EHEC are themselves known to encode several effectors which have GEF activity(16-18). However, whether these contribute to the GTPase activation required for EspG-dependent hijacking of PAK, or whether some other host or

pathogen factor is responsible, is unknown. Here, we sought to determine how EPEC ensures a sufficient level of Rho GTPase activation in target host cells.

EPEC activates Rho GTPases

To determine the source of the active Rho GTPases required for EPEC to hijack host PAK(10), we first sought to determine whether the level of active GTPases changes in response to infection. EPEC-infected cell lysates were incubated with GST-PAK-PBD beads, which specifically interact with the active form of Rac1 and Cdc42. EPEC infection resulted in significant GTPase activation, similar to that seen upon control infection with *Salmonella* (Figure 1A, S1A). In contrast, infection with *⊿escN* EPEC, which lack a functional type 3 secretion system, triggered negligible GTPase activation, suggesting that an EPEC-delivered effector is responsible for triggering activation.

The EPEC effector Map (mitochondria associated protein) is known to be a GEF for Cdc42, and indeed has been shown to trigger Cdc42-dependent filopodia formation upon EPEC infection(19, 20). However unlike *ΔespG* EPEC*, Δmap* EPEC showed no defect in either pedestal formation (Figure 1B,C) or attachment to cultured Hap1 cells (Figure 1D). A double *ΔespGΔmap* strain displayed no additional defect in either phenotype when compared to *ΔespG* EPEC, suggesting that Map is not required to activate the GTPases necessary for the hijacking of PAK and consequent pedestal formation. Indeed, in our cell culture infection model Δ*map* EPEC activated Rho GTPases equivalently to WT (Figure 1E, S1B), However to our surprise, control *ΔespG* EPEC were unable to induce GTPase activation. Similar results were observed in multiple cell lines (Figure S1C,D,E). In some cell types (Caco-2 and LoVo) the level of Cdc42 activation was lower in cells infected with Δ*map* EPEC than those infected with WT, suggesting that Map does play a role in Cdc42 activation. However in all cases, this reduction was much smaller than that seen in cells infected with either Δ*espG* EPEC or the *ΔespGΔmap* strain, in which Cdc42 activation was abolished. As EspG has no structural or sequence similarity to known GEFs, and has never been reported to possess GEF activity, this suggests that EPEC may exploit a host cell GEF to induce the GTPase activity required for EspG-

mediated hijacking of PAK, and that seemingly EspG itself plays a key role in this process.

EPEC recruits a host Cdc42 GEF to induce GTPase activation

PAK function in cells requires Rho GTPases(21), but PAK can also itself promote activation of GTPases, for example via PIX (PAK-interacting exchange factor)(22), leading to amplification of PAK signaling. It is therefore possible that the EspG-dependent increase in active Rho GTPases upon EPEC infection is due to EspG hijacking the PAK cascade. To test this possibility, we performed a GTPase activation assay in HAP1 cells infected with *ΔespG* EPEC complemented with various derivatives of EspG (Figure 2A, S2A). Complementation with WT EspG restored the ability of *ΔespG* EPEC to activate Cdc42, whereas derivatives deficient in binding to Arf GTPases alone, or to both Arf and PAK, were unable to restore Rho activation. This is presumably because the interaction with Arf GTPases is required for correct localization of EspG. Mutations that disrupt the binding of EspG to either Rab GTPases (ΔR*)* or PAK (ΔP) did not affect Rho GTPase activation, suggesting that EspG can signal to Rho proteins independently of PAK, and therefore also PIX. In confirmation of this, Cdc42 was efficiently activated by EPEC in either ΔPAK1 cells, or ΔPAK1 cells treated with a chemical inhibitor of other Class I PAK isoforms (FRAX486) (Figure 2B, S2B).

In order to identify the signaling network that leads to GTPase activation, we attempted to reconstitute EspG signaling *in vitro* using lipid bilayer-coated silica microspheres incubated in cell-free porcine brain extract. As we have previously shown, EspG anchored to microspheres coated with PC:PS (phosphatidylcholine:phosphatidylserine) bilayers fails to recruit any PAK, and also fails to recruit any endogenous Cdc42 (Figure 2C). Lipid bilayers designed to further mimic the site of action of EspG by including PIP2 (phosphatidylinositol 4,5 bisphosphate), known to be enriched at sites of EPEC attachment to host cells(23), recruited active, phosphorylated PAK (PAK-P) and a small amount of Cdc42. This was significantly enhanced by the presence of EspG, which lead to efficient recruitment of both Cdc42 and phosphorylated PAK (Figure 2C). This confirms that EspG can trigger recruitment and activation of Cdc42, and suggests that membrane lipid composition is of critical importance in this EspG-mediated signaling to GTPases.

To attempt to identify how EspG signals to Rho GTPases, the proteins recruited from porcine brain extracts to PC:PS:PIP2-coated microspheres in the presence and absence of anchored EspG were separated by SDS-PAGE (Fig 2D) and identified by parallel mass spectrometry (Table S1). The top hits are summarized in Fig 2E. Of particular note, one of the proteins enriched in the presence of EspG was a Cdc42-specific GEF, Frabin (also known as FGD4, FYVE, RhoGEF And PH Domain Containing 4)(24, 25). The recruitment of Frabin was further confirmed using immunoblotting (Figure 2F).

We next examined whether Frabin plays a role in EPEC attachment and pedestal formation. In contrast to WT Hap1 cells, when Frabin knockout Hap1 cells (ΔFrabin) were infected with WT EPEC, virtually no increase was seen in the level of active Cdc42 (Figure 3A, S3A). The level of active, phosphorylated PAK induced by EPEC infection was also much lower in ΔFrabin than WT cells (Figure 3B, S3B). There was still a residual level of PAK phosphorylation triggered in ΔFrabin cells; as Frabin is a Cdc42-specific GEF this may be due to Rac1 activation, triggered by a separate pathway. Consistent with this, treatment of ΔFrabin cells with a Rac1 inhibitor (EHT1864) completely abolished EPEC-induced phosphorylation of PAK, whereas PAK phosphorylation was only partially reduced in WT Hap1 cells (Fig 3B, S3B). Pedestals formed by WT EPEC on ΔFrabin cells were less efficient in terms of actin recruitment and had a different morphology compared to those formed on control HAP1 cells (Figure 3C). Both pedestal length (Figure 3D) and bacterial attachment (Figure 3E) were significantly impaired by either knockdown or knockout of Frabin. An equivalent reduction in EPEC attachment was observed in HeLa, Caco-2 and LoVo cells treated with Frabin siRNA (Figure S3C,D). As seen for PAK phosphorylation above, pedestal length and bacterial attachment showed a small further decrease upon inhibition of Rac1 in ΔFrabin cells, and only a partial reduction in WT Hap1 cells (Figure 3D and 3E). Collectively, this data shows that EPEC generates the level of active Cdc42 in infected cells required for subsequent hijacking of PAK via the host GEF Frabin.

The DH and PH domains of Frabin are essential for Rho GTPase activation by EPEC

Frabin consists of multiple functional domains (Figure 4A)(26). At the N-terminus is an actin-binding domain (ABD), followed by a Dbl-homology domain (DH) that possess GEF activity, a lipid-binding plekstrin-homolgy domain (PH), a phosphatidylinositol-binding Fab1, YOTB, Vac1 and EEA1 domain (FYVE) and finally a second PH domain. To determine which functional domains of Frabin are required for EPEC pedestal formation, we generated a series of derivative versions corresponding to various combinations of the individual domains (Figure 4A), and expressed these in ΔFrabin cells, prior to infection with EPEC. The ABD, FYVE and both PH domains could all be deleted without impacting the EPEC-triggered Cdc42 activation (Figure 4B, S4A). Perhaps unsurprisingly, the minimum required for GTPase activation was the DH, i.e. the site of GEF activity. However, the DH domain was inactive when fused to the ABD alone (Figure 4B, S4A; pFrabin$^{1-392}$). This could be due to the ABD sequestering this construct to actin filaments, away from the plasma membrane where Rho GTPases are enriched. Indeed, Cdc42 activation was restored when a phospholipid-binding PH domain was also present (Figure 4B, S4A; pFrabin$^{1-523}$).

All of the Frabin constructs that were competent for EPEC-induced Cdc42 activation (Figure 4B) were also able to promote PAK activation (Figure 4C, S4B), with the exception of the DH domain alone (pFrabin$^{210-392}$). As PAK activation could be triggered by the DH-PH domain combination (pFrabin$^{210-523}$), this suggests that although the GEF domain alone is able to activate Cdc42 within the cell, the activation must occur at a specific subcellular location for PAK to be activated. Frabin constructs that were able to restore PAK activation in ΔFrabin cells were also able to restore pedestal formation (Figure 4D) and bacterial attachment (Figure 4E). Collectively this demonstrates that Frabin is responsible for EPEC-induced Cdc42 activation, via its DH domain, and that the presence of the PH domain is required to ensure that this Cdc42 activation occurs in the correct location within the cell to allow PAK activation and consequent bacterial attachment to the host cell.

Presumably, once pedestals have been produced the Frabin pathway may be switched off. Consistent with this, the levels of active Cdc42 are approximately 50% lower at 4 hours compared to 1 hour post-infection (Figure S4C). Intriguingly, EPEC

encodes an effector, EspH, that can inhibit certain mammalian GEFs(27, 28). Transfection of HAP1 cells with a plasmid expressing EspH abolished EPEC-induced Cdc42 activation at all time points (Figure 4F, S4C), suggesting it could play a role in down-regulating the Frabin pathway following pedestal production.

PIP2 and Arf6 are required to localize Frabin

The first Frabin PH domain, required for EPEC to able to activate PAK, is known to bind to phosphatidylinositol 4,5 bisphosphate (PIP2), though it's binding specificity remains unclear(29). PIP2 was present in the lipid bilayer-coated microspheres used to identify Frabin as a target for EspG (Figure 2), and is known to be enriched at sites of EPEC pedestal formation(23). Consistent with the role of the PH domain, Frabin co-localised with PIP2, immediately below sites of EPEC attachment to cultured Hap1 cells (Figure 5A). In the absence of EspG, although PIP2 was present at sites of EPEC attachment, Frabin was not recruited (Figure 5A). When Hap1 cells were infected with EPEC that expresses Tir^{Y474A}, a strain which attaches but is unable to generate actin pedestals, both PIP2 and frabin were still recruited to sites of bacterial adhesion (Figure 5A), suggesting that actin polymerization is not required for Frabin recruitment by EspG.

As EspG is required for Frabin association with sites of EPEC attachment, we sought to determine whether EspG directly interacts with Frabin by reconstituting Frabin recruitment to lipid bilayers using purified recombinant proteins. Microspheres coated with a bilayer composed of phosphatidylcholine and phosphatidylinositol (PC:PI), and anchored with EspG and constitutively-active $Arf6^{QL}$ (required for EspG membrane association) showed minimal recruitment of Frabin, with bound Frabin only visible when present at high concentrations (Figure 5B). Recombinant Frabin could be efficiently recruited however when EspG and $Arf6^{QL}$ were anchored to bilayers also containing PIP2, but not to control PIP2 microspheres in the absence of $Arf6^{QL}$ and EspG. Surprisingly, Frabin was also recruited, though less efficiently, to control $Arf6^{QL}$ PIP2 microspheres, though not to inactive, GDP-bound Arf6 (Figure 5B).

It is therefore possible that active Arf6 and PIP2 are responsible for Frabin enrichment at sites of EPEC attachment and that, as EspG is known to prevent cellular Arf GAPs from inactivating Arfs(30), the role of EspG is to enhance the local

level of active Arf. Alternatively, it is possible that Frabin is able to directly interact with either Arf6 or EspG. As Arf6 is required for anchoring EspG to lipid bilayers in our *in vitro* reconstitution system, we returned to cell infection to further test the role of EspG. When ΔespG EPEC were used to infect Hap1 cells transfected with $EspG^{\Delta A}$ (a derivative incapable of binding Arfs and therefore unable to localise to the host cell membrane), Frabin was not significantly enriched at sites of bacterial attachment (Fig 5C). However, when $EspG^{\Delta A}$ is artificially targeted to the membrane by fusing to a lipid-binding PH domain (PH-$EspG^{\Delta A}$), Frabin was efficiently recruited to sites of EPEC attachment. This suggests that EspG can enhance recruitment of Frabin without interacting with Arf6, and therefore does not act to simply protect active Arf6 from inactivation.

Discussion

Collectively, the results presented here allow us to propose a model by which EPEC ensures that target cells contain the high levels of localized active Rho GTPases necessary for subversion of PAK signaling (Figure 5D). Upon injection by the T3SS, EspG forms a complex with active, GTP-bound Arf6 at the plasma membrane. EspG binding sterically blocks cellular Arf GAPs from binding and inactivating Arf6. The initial attachment of EPEC leads to the accumulation of PIP2 directly beneath the adherent bacteria. The coincident PIP2 and EspG-Arf6 lead to enrichment of Frabin, triggering local activation of Cdc42. This in turn leads to activation of PAK, which is hijacked by EspG-Arf6 to promote the actin rearrangements necessary for pedestal formation and intimate EPEC attachment to the host cell.

Active Rho GTPases are a requirement for exploitation of PAK by EPEC(10). Rho GTPases are master regulators of multiple signaling pathways within eukaryotic cells, and consequently their activation status is spatially and temporally dynamic(11). If EPEC encounters a cell in which these pathways are already active, which in cell culture may depend on specific cell line and growth conditions, the Frabin pathway may not be as important for pedestal generation. This possibly explains why previous studies have failed to identify a role for Rho GTPases in pedestal formation(31). However, when needed, by promoting Frabin activation directly beneath adherent bacteria, EPEC ensures that local PAK will always be in the GTPase-activated state required for EspG hijacking.

Little is known about the function of Frabin in healthy cells. Various mutations in the Frabin gene have been linked to the hereditary neuropathy Charcot-Marie-Tooth disease(32), and Frabin may play a role in myelin homeostasis in the peripheral nervous system(33). Frabin overexpression may also play a role in certain cancers(34). The presence of three potential lipid-binding domains (two PH domains and a FYVE domain), and an actin-binding domain suggest it is able to localize to various sites within the cell to perform multiple functions(29), and indeed Frabin has been seen to localize to several actin-associated membrane structures(35). Here we show that the role of Frabin in EPEC pedestal formation requires only the DH (GEF) domain and the first PH domain. PH domains are found in many proteins and are known to target cellular membranes by binding to phosphoinositide lipids and proteins(36). Indeed, some PH domains are able to bind to both lipids and small GTPases, and have been reported to act as coincidence detectors(37). For example, Fapp1 (four-phosphate adaptor protein 1) is targeted to membranes by the its PH domain, which detects coincident Arf1 and phosphatidylinositol-4-phosphate(38).

Frabin enrichment at sites of EPEC attachment also seems to require two coincident signals. The first of these, PIP2, is known to be enriched directly beneath the adherent bacteria(23). Indeed, disruption of this PIP2 accumulation was shown previously to severely impair EPEC attachment and actin pedestal formation(23), which the results presented here suggest may be at least in part due to impaired Frabin localization. The second required signal for Frabin recruitment could be supplied by constitutively-activeArf6^{QL} *in vitro* using purified proteins (Fig 5B), but during cell infection EspG was necessary (Fig 5A). As EspG is known to interact with Arfs and protect them from inactivation(30), the requirement for EspG could be due to it enhancing the level of active Arf present at the site of bacterial attachment. However as a mutant of EspG unable to interact with Arfs could efficiently recruit Frabin when artificially targeted to the membrane, it is possible that EspG can directly interact with Frabin. Nevertheless, during infection with WT EPEC, EspG localises to bacterial attachment sites by binding Arf6, and thus both potential Frabin interactors are present together and may well cooperate. It should also be noted recruitment to membranes does not necessarily correlate with activation of Frabin's GEF activity (i.e. the DH domain), and the requirement of EspG for Cdc42 activation may be indicative of a direct role in activating Frabin.

The molecular details of the complex interactions regulating this pathway will require further study, but we have identified Frabin as a key component of the signaling complex assembled by EspG to ensure that conditions within the target cell are permissive for EPEC to form actin pedestals. This is the first report of Frabin being involved in bacterial pathogenesis. Previously, Frabin has been shown to be required for the entry of the intracellular parasite *Cryptosporidum parvum* into epithelial cells, by promoting Cdc42 activation and consequent downstream actin rearrangements(39). Though the molecular details of this pathway remain unknown, as seen here with EPEC the recruitment of Frabin by *C. parvum* required the generation of phosphorylated phosphoinositide lipids in the target cell membrane. Epstein-Barr virus also subverts Frabin, leading to Cdc42 activation and enhanced motility of virus-infected cells(40). Rho GTPases such as Cdc42 are ubiquitous targets for pathogenic bacteria due to their central role in myriad cell signaling pathways(41). Likewise, many bacteria manipulate phosphoinositide lipids in target cell membranes(42). It is thus intriguing to speculate that Frabin may be an important component of the signaling networks subverted by other pathogens to drive the cytoskeletal changes underlying pathogenesis.

Materials and methods

Bacterial strains

EPEC E2348/69, isogenic mutant EPEC Δ*espG1*/Δ*espG2* (Prof. Feng Shao) and EPEC Δ*map* (Gad Frankel) were generous gifts.

Plasmids

The plasmids pTrcEspG, pTrcEspGΔR, pTrcEspGΔP, pTrcEspGΔAP, pTrcEspGΔA, pCDNA-HA-EspGΔA and pCDNA-HA-PH-EspGΔA were described previously(10, 43). Plasmids pET20b-Arf6, pET15b-espG, pET20b-Frabin, pCDNAnHA-Frabin^{WT}, pCDNAnHA-Frabin$^{(1\text{-}150)}$, pCDNAnHA-Frabin$^{(1\text{-}392)}$, pCDNAnHA-Frabin$^{(1\text{-}523)}$, pCDNAnHA-Frabin$^{(210\text{-}523)}$, pCDNAnHA-Frabin$^{(210\text{-}392)}$ and pCDNAnHA-Frabin^{L23R} were generated using Gateway methodology (Invitrogen).

Antibodies

Antibodies were supplied by the following: Cell Signaling Technology (Phospho-PAK1 (Ser144)/PAK2 (Ser141), #2606; PAK1, #2602); Santacruz Biotechnology (Frabin, Sc-136333); Abcam (Rac1, ab33186; Arf6, ab81650; Tubulin, ab7291); Sigma (Actin, A2066); BD Bioscience (Cdc42, #610929); QIAGEN (His Tag, 34660).

Rabbit anti-intimin was raised against full-length recombinant initimin by Diagnostics Scotland.

Mammalian cell culture and transfection

The WT Hap1 cells (C631) and verified knockout lines ΔArf6 (HZGHC003403c006), ΔFrabin (HZGHC004680c010) and ΔPak1 (HZGHC000160c012) were purchased from Horizon Discovery. Cells were maintained in IMDM supplemented with 10% FBS, 100 U/mL penicillin-streptomycin. Where indicated, cells were pre-incubated for 60 minutes prior to bacterial infection with 10 μM of the inhibitor EHT1864 (Merck) or 25 μM PAK inhibitor (FRAX486, Tocris).

Where indicated, plasmids were introduced into mammalian cells using the Neon transfection system (Invitrogen) according to the manufacturer's instructions.

Flexitube siRNAs (Qiagen) used to knockdown Frabin (Hs_FGD4_1 NM_139241 and Hs_FGD4_2 NM_139241) were transfected using Oligofectamine (Life Technologies) following the manufacturer's instructions.

Attachment assay and pedestal quantification

Cells were infected as described previously(44). For pedestal quantification cells were washed three times with PBS, fixed and stained with Alexa Fluor 488 phalloidin (Lifetech) to visualise actin and an anti-intimin antibody to visualise the bacteria. The number of actin pedestals per cell were then counted using fluorescence microscopy. For adhesion assays, after infection, cells were washed twice with PBS then twice briefly with 200 mM Glycine (pH 2), followed by a further two washes with PBS. Cells were fixed and stained as above, and the number of bacteria still adherent counted using microscopy.

The pedestal length was determined by drawing a line beneath the attached bacteria and measuring the length using ImageJ (FIJI) tool. A minimum of 150 attached bacteria were counted per condition to estimate the average pedestal length for a given condition. Pixel (fluorescence) intensity plots were generated using "plot profile" tool of the ImageJ (FIJI) and the lines were drawn through pedestal or pedestal forming regions.

GST-PBD GTPase activation assay

Active GTPases were detected as described previously(45). Briefly, indicated cells were washed twice in ice cold PBS, then lysed in RIPA buffer (Sigma Aldrich) supplemented with a cocktail of protease inhibitors. Cell lysates were subjected to centrifugation (13,000xg, 15 mins, 4 ˚C) to remove insoluble material. Equivalent

amounts of cleared lysates were then incubated with GST-PBD bound to glutathione-sepharose resin (GE Healthcare) at 4˚C for 30 minutes. Resin was packed onto a column, extensively washed, and then bound Cdc42 and Rac1 eluted using SDS-urea. The samples were then analysed using SDS-PAGE and Western blotting.

***In vitro* pull-down assays**

Pull downs were performed as previously(46). Briefly, silica microspheres (Bangs Laboratories) were coated with a bilayer composed of either phosphatidylcholine (PC) and phosphatidylserine (PS), at a molar ratio of 80:20 PC:PS, or phosphatidylcholine (PC), phosphatidylinositol (PI) and phosphatidylinositol 4,5 bisphosphate (PIP2), at a 48:48:4 molar ratio of PC:PI:PIP2. All lipids were purchased from Avanti Polar Lipids. Indicated proteins were anchored to these bilayers, prior to incubation in cell-free porcine brain extract. Following incubation for 15 minutes, bilayers were washed extensively and associated proteins analysed by SDS-PAGE. To identify recruited proteins, beads were washed with 50 mM ammonium bicarbonate (pH 8.5) supplemented with 0.5 mM DTT and then were incubated with trypsin. The digested proteins were identified by electrospray ionization liquid chromatography mass spectrometry (Mass Spectrometry Service, Cambridge Centre for Proteomics, University of Cambridge, Cambridge, UK). The MS fragmentation data were used to search the National Center for Biotechnology Information (NCBI) database using the MASCOT search engine (www.matrixscience.com).

PAK activation assays

PAK activation was measured as previously described(10). Briefly, cells were cultured in 10 cm dishes, and starved in serum-free IMDM overnight. The following day cells were infected (90 mins) or treated with appropriate drugs, as indicated, and then washed twice with PBS before being detached using a cell scraper and resuspended in SDS-UREA. Samples were analyzed by SDS-PAGE and immunoblotting using appropriate antibodies. Immunoblots are representative of at least three separate repeats. Bands were visualized using a LI-COR Odyssey Fc imaging system, and band intensities were quantified using the LI-COR Image Studio software.

Acknowledgements

We thank Rachael Stone for technical assistance. This work was funded by a Wellcome Trust Senior Investigator Award (101828/Z/13/Z), by the Medical Research Council (MR/L008122/1) and by the Cambridge Isaac Newton Trust.

References

1. Hu J, Torres AG. 2015. Enteropathogenic Escherichia coli: foe or innocent bystander? Clin Microbiol Infect 21:729-34.
2. Marder Mph EP, Griffin PM, Cieslak PR, Dunn J, Hurd S, Jervis R, Lathrop S, Muse A, Ryan P, Smith K, Tobin-D'Angelo M, Vugia DJ, Holt KG, Wolpert BJ, Tauxe R, Geissler AL. 2018. Preliminary Incidence and Trends of Infections with Pathogens Transmitted Commonly Through Food - Foodborne Diseases Active Surveillance Network, 10 U.S. Sites, 2006-2017. MMWR Morb Mortal Wkly Rep 67:324-328.
3. Ochoa TJ, Contreras CA. 2011. Enteropathogenic escherichia coli infection in children. Curr Opin Infect Dis 24:478-83.
4. Nguyen Y, Sperandio V. 2012. Enterohemorrhagic E. coli (EHEC) pathogenesis. Front Cell Infect Microbiol 2:90.
5. Croxen MA, Finlay BB. 2010. Molecular mechanisms of Escherichia coli pathogenicity. Nat Rev Microbiol 8:26-38.
6. Lai Y, Rosenshine I, Leong JM, Frankel G. 2013. Intimate host attachment: enteropathogenic and enterohaemorrhagic Escherichia coli. Cell Microbiol 15:1796-808.
7. Sanger JM, Chang R, Ashton F, Kaper JB, Sanger JW. 1996. Novel form of actin-based motility transports bacteria on the surfaces of infected cells. Cell Motil Cytoskeleton 34:279-87.
8. Velle KB, Campellone KG. 2017. Extracellular motility and cell-to-cell transmission of enterohemorrhagic E. coli is driven by EspFU-mediated actin assembly. PLoS Pathog 13:e1006501.
9. Wong AR, Pearson JS, Bright MD, Munera D, Robinson KS, Lee SF, Frankel G, Hartland EL. 2011. Enteropathogenic and enterohaemorrhagic Escherichia coli: even more subversive elements. Mol Microbiol 80:1420-38.
10. Singh V, Davidson A, Hume PJ, Koronakis V. 2019. Pathogenic Escherichia coli Hijacks GTPase-Activated p21-Activated Kinase for Actin Pedestal Formation. mBio 10.
11. Hall A. 2012. Rho family GTPases. Biochem Soc Trans 40:1378-82.
12. Lemichez E, Aktories K. 2013. Hijacking of Rho GTPases during bacterial infection. Exp Cell Res 319:2329-36.
13. Aktories K. 2011. Bacterial protein toxins that modify host regulatory GTPases. Nat Rev Microbiol 9:487-98.
14. Bulgin R, Raymond B, Garnett JA, Frankel G, Crepin VF, Berger CN, Arbeloa A. 2010. Bacterial guanine nucleotide exchange factors SopE-like and WxxxE effectors. Infect Immun 78:1417-25.
15. Fu Y, Galan JE. 1999. A salmonella protein antagonizes Rac-1 and Cdc42 to mediate host-cell recovery after bacterial invasion. Nature 401:293-7.

16. Bulgin RR, Arbeloa A, Chung JC, Frankel G. 2009. EspT triggers formation of lamellipodia and membrane ruffles through activation of Rac-1 and Cdc42. Cell Microbiol 11:217-29.
17. Kenny B, Jepson M. 2000. Targeting of an enteropathogenic Escherichia coli (EPEC) effector protein to host mitochondria. Cell Microbiol 2:579-90.
18. Arbeloa A, Bulgin RR, MacKenzie G, Shaw RK, Pallen MJ, Crepin VF, Berger CN, Frankel G. 2008. Subversion of actin dynamics by EspM effectors of attaching and effacing bacterial pathogens. Cell Microbiol 10:1429-41.
19. Kenny B, Ellis S, Leard AD, Warawa J, Mellor H, Jepson MA. 2002. Co-ordinate regulation of distinct host cell signalling pathways by multifunctional enteropathogenic Escherichia coli effector molecules. Mol Microbiol 44:1095-1107.
20. Berger CN, Crepin VF, Jepson MA, Arbeloa A, Frankel G. 2009. The mechanisms used by enteropathogenic Escherichia coli to control filopodia dynamics. Cell Microbiol 11:309-22.
21. Manser E, Leung T, Salihuddin H, Zhao ZS, Lim L. 1994. A brain serine/threonine protein kinase activated by Cdc42 and Rac1. Nature 367:40-6.
22. Manser E, Loo TH, Koh CG, Zhao ZS, Chen XQ, Tan L, Tan I, Leung T, Lim L. 1998. PAK kinases are directly coupled to the PIX family of nucleotide exchange factors. Mol Cell 1:183-92.
23. Sason H, Milgrom M, Weiss AM, Melamed-Book N, Balla T, Grinstein S, Backert S, Rosenshine I, Aroeti B. 2009. Enteropathogenic Escherichia coli subverts phosphatidylinositol 4,5-bisphosphate and phosphatidylinositol 3,4,5-trisphosphate upon epithelial cell infection. Mol Biol Cell 20:544-55.
24. Obaishi H, Nakanishi H, Mandai K, Satoh K, Satoh A, Takahashi K, Miyahara M, Nishioka H, Takaishi K, Takai Y. 1998. Frabin, a novel FGD1-related actin filament-binding protein capable of changing cell shape and activating c-Jun N-terminal kinase. J Biol Chem 273:18697-700.
25. Umikawa M, Obaishi H, Nakanishi H, Satoh-Horikawa K, Takahashi K, Hotta I, Matsuura Y, Takai Y. 1999. Association of frabin with the actin cytoskeleton is essential for microspike formation through activation of Cdc42 small G protein. J Biol Chem 274:25197-200.
26. Nakanishi H, Takai Y. 2008. Frabin and other related Cdc42-specific guanine nucleotide exchange factors couple the actin cytoskeleton with the plasma membrane. J Cell Mol Med 12:1169-76.
27. Dong N, Liu L, Shao F. 2010. A bacterial effector targets host DH-PH domain RhoGEFs and antagonizes macrophage phagocytosis. EMBO J 29:1363-76.
28. Wong AR, Clements A, Raymond B, Crepin VF, Frankel G. 2012. The interplay between the Escherichia coli Rho guanine nucleotide exchange factor effectors and the mammalian RhoGEF inhibitor EspH. mBio 3.
29. Eitzen G, Smithers CC, Murray AG, Overduin M. 2019. Structure and function of the Fgd family of divergent FYVE domain proteins (1). Biochem Cell Biol 97:257-264.
30. Selyunin AS, Reddick LE, Weigele BA, Alto NM. 2014. Selective protection of an ARF1-GTP signaling axis by a bacterial scaffold induces bidirectional trafficking arrest. Cell Rep 6:878-91.
31. Ben-Ami G, Ozeri V, Hanski E, Hofmann F, Aktories K, Hahn KM, Bokoch GM, Rosenshine I. 1998. Agents that inhibit Rho, Rac, and Cdc42 do not

block formation of actin pedestals in HeLa cells infected with enteropathogenic Escherichia coli. Infect Immun 66:1755-8.
32. Delague V, Jacquier A, Hamadouche T, Poitelon Y, Baudot C, Boccaccio I, Chouery E, Chaouch M, Kassouri N, Jabbour R, Grid D, Megarbane A, Haase G, Levy N. 2007. Mutations in FGD4 encoding the Rho GDP/GTP exchange factor FRABIN cause autosomal recessive Charcot-Marie-Tooth type 4H. Am J Hum Genet 81:1-16.
33. Horn M, Baumann R, Pereira JA, Sidiropoulos PN, Somandin C, Welzl H, Stendel C, Luhmann T, Wessig C, Toyka KV, Relvas JB, Senderek J, Suter U. 2012. Myelin is dependent on the Charcot-Marie-Tooth Type 4H disease culprit protein FRABIN/FGD4 in Schwann cells. Brain 135:3567-83.
34. Bossan A, Ottman R, Andl T, Hasan MF, Mahajan N, Coppola D, Chakrabarti R. 2018. Expression of FGD4 positively correlates with the aggressive phenotype of prostate cancer. BMC Cancer 18:1257.
35. Kim Y, Ikeda W, Nakanishi H, Tanaka Y, Takekuni K, Itoh S, Monden M, Takai Y. 2002. Association of frabin with specific actin and membrane structures. Genes Cells 7:413-20.
36. Scheffzek K, Welti S. 2012. Pleckstrin homology (PH) like domains - versatile modules in protein-protein interaction platforms. FEBS Lett 586:2662-73.
37. Carlton JG, Cullen PJ. 2005. Coincidence detection in phosphoinositide signaling. Trends Cell Biol 15:540-7.
38. Liu Y, Kahn RA, Prestegard JH. 2014. Interaction of Fapp1 with Arf1 and PI4P at a membrane surface: an example of coincidence detection. Structure 22:421-30.
39. Chen XM, Splinter PL, Tietz PS, Huang BQ, Billadeau DD, LaRusso NF. 2004. Phosphatidylinositol 3-kinase and frabin mediate Cryptosporidium parvum cellular invasion via activation of Cdc42. J Biol Chem 279:31671-8.
40. Liu HP, Chen CC, Wu CC, Huang YC, Liu SC, Liang Y, Chang KP, Chang YS. 2012. Epstein-Barr virus-encoded LMP1 interacts with FGD4 to activate Cdc42 and thereby promote migration of nasopharyngeal carcinoma cells. PLoS Pathog 8:e1002690.
41. Lemichez E. 2017. New Aspects on Bacterial Effectors Targeting Rho GTPases. Curr Top Microbiol Immunol 399:155-174.
42. Walpole GFW, Grinstein S, Westman J. 2018. The role of lipids in host-pathogen interactions. IUBMB Life 70:384-392.
43. Humphreys D, Singh V, Koronakis V. 2016. Inhibition of WAVE Regulatory Complex Activation by a Bacterial Virulence Effector Counteracts Pathogen Phagocytosis. Cell Rep 17:697-707.
44. Smith K, Humphreys D, Hume PJ, Koronakis V. 2010. Enteropathogenic Escherichia coli recruits the cellular inositol phosphatase SHIP2 to regulate actin-pedestal formation. Cell Host Microbe 7:13-24.
45. Benard V, Bohl BP, Bokoch GM. 1999. Characterization of rac and cdc42 activation in chemoattractant-stimulated human neutrophils using a novel assay for active GTPases. J Biol Chem 274:13198-204.
46. Koronakis V, Hume PJ, Humphreys D, Liu T, Horning O, Jensen ON, McGhie EJ. 2011. WAVE regulatory complex activation by cooperating GTPases Arf and Rac1. Proc Natl Acad Sci U S A 108:14449-54.

Figure legends

Figure 1. EPEC activates Cdc42 upon attachment to host cells.

(**A**) Immunoblot of the level of Cdc42 and Rac1 isolated by GST-GBD beads ("active") from lysates prepared from either uninfected Hap1 cells, or those infected with WT *Salmonella,* WT EPEC or Δ*escN* EPEC, as indicated. Also shown is the total level of Cdc42 and Rac1 (active and inactive) in the lysates ("total") . (**B**) Fluorescence microscopy images of actin pedestals formed on Hap1 cells by WT, Δ*espG*, Δ*map* and Δ*espG*Δ*map* EPEC bacteria at 60 mins post infection. Actin (green) is stained with Alexa Fluor 488-phalloidin, and bacteria (red) are stained with anti-intimin antibody. Scale bar, 1 μm. (**C**) Average pedestal length produced by EPEC strains as described in (B). Each bar represents the average of results from 3 separate experiments (100 to 200 cells for each replicate, 300-500 cells in total). (**D**) Quantification of the attachment of strains described in (B) to WT Hap1 cells, relative to that of WT EPEC (there are typically 6 to 7 WT EPEC bacteria per cell). Error bars indicate SD. ***, $P < 0.001$; ns, not significant (by one-way analysis of variance [ANOVA] followed by a *post hoc* Dunnett comparison) relative to WT EPEC attachment. (**E)** Immunoblot of the level of Cdc42 and Rac1 isolated by GST-GBD beads ("active") from lysates prepared from either uninfected Hap1 cells, or those infected with WT EPEC*,* Δ*espG* EPEC or Δ*map* EPEC, as indicated. Also shown is the total level of Cdc42 and Rac1 in the lysates ("total").

Figure 2. EPEC recruits the cdc42 GEF Frabin.

(**A**) Immunoblot of the level of Cdc42 isolated by GST-GBD beads ("active") from lysates prepared from Hap1 cells infected with the indicated EPEC strains. Also shown is the total level of Cdc42 in the lysates ("total"). (**B**) Immunoblot of the level of Cdc42 isolated by GST-GBD beads ("active") from lysates prepared from either uninfected WT Hap1 cells, or EPEC-infected WT HAP1, ΔPAK1 Hap1 or ΔPAK1 cells pre-treated with PAK inhibitor, as indicated. (**C**) Immunoblot showing recruitment of the indicated proteins from porcine brain extract by PC:PI or PC:PI:PIP2 ("PIP2") lipid bilayers in the absence or presence of EspG. (**D**) SDS/PAGE analysis and Coomassie blue staining of proteins recruited by PC:PI and PC:PI:PIP2 ("PIP2") lipid bilayers from porcine brain extract in presence and

absence of EspG. (**E**) Table showing top hits from mass spectrometry analysis of specific proteins recruited by PC:PI:PIP2 bilayers in presence of EspG. (**F**) Immunoblot showing the levels of indicated proteins in samples from (D).

Figure 3. Frabin is important for EPEC pedestal and attachment.

(**A**) Immunoblot of the level of Cdc42 isolated by GST-GBD beads ("active") from lysates prepared from either uninfected WT Hap1, or EPEC-infected WT or ΔFrabin Hap1 cells. Also shown is the total level of Cdc42 in the lysates ("total"). (**B**) Immunoblot of the level of total (PAK) and active (phosphorylated on serine 144; PAK-P) PAK in uninfected WT Hap1 cells, and EPEC-infected WT or ΔFrabin cells, with and without pretreatment with Rac inhibitor EHT 1864. (**C**) Fluorescence microscopy images of actin pedestals formed by WT EPEC on WT or ΔFrabin HAP1 cells, with and without pretreatment with Rac inhibitor EHT 1864. Actin (green) is stained with Alexa Fluor 488-phalloidin, and bacteria (red) are stained with anti-intimin antibody. Scale bar, 1 μm. (**D**) Average pedestal length formed by WT EPEC on cells described in (C). (**E**) Quantification of the attachment of EPEC to cells as in (C), relative to that of WT EPEC attachment on WT HAP1 cells (there are typically 6 to 7 WT EPEC bacteria per WT HAP1 cell). Each bar represents the average of results from 3 separate experiments (100 to 200 cells for each replicate, 300-500 cells in total). Error bars indicate SD. ***, $P < 0.001$; **, $P < 0.05$; ns, not significant (by one-way analysis of variance [ANOVA] followed by a *post hoc* Dunnett comparison) relative to attachment on WT HAP1 cells.

Figure 4. DH-PH1 domains of Frabin are sufficient for pedestal assembly.

(**A**) Schematic showing the domain architecture of Frabin and the various derivative constructs used here. (**B**) Immunoblot of the level of Cdc42 isolated by GST-GBD beads ("active") from lysates prepared from ΔFrabin HAP1 cells transfected with the indicated Frabin constructs and infected with WT EPEC. Also shown is the total level of Cdc42 in the lysates ("total"). (**C**) Immunoblot of the level of total (PAK) and active (phosphorylated on serine 144; PAK-P) PAK in ΔFrabin HAP1 cells transfected with the indicated Frabin constructs and infected with WT EPEC. (**D**) Fluorescence microscopy images of actin pedestals formed on ΔFrabin HAP1 cells either

untransfected (control) or transfected with the indicated Frabin constructs. Actin (red) is stained with Texas red-phalloidin, and bacteria (blue) are stained with anti-intimin antibody, frabin constructs (green). Scale bar, 10 μm. Insets magnify the highlighted area. (**E**) Quantification of the attachment of WT EPEC to Δ Frabin cells transfected with the indicated Frabin constructs, relative to attachment of WT EPEC to Wt HAP1 cells (there are typically 6 to 7 WT EPEC bacteria per WT HAP1 cell). Each bar represents the average of results from 3 separate experiments (100 to 200 cells for each replicate, 300-500 cells in total). Error bars indicate SD. **, $P < 0.05$; ns, not significant (by one-way analysis of variance [ANOVA] followed by a *post hoc* Dunnett comparison) relative to WT EPEC attachment. (**F**) Immunoblot of the level of Cdc42 isolated by GST-GBD beads ("active") from lysates prepared from either untransfected (control) WT Hap1 cells, or those transfected with a plasmid expressing EspH (pEspH). Cells were either uninfected (-) or infected with WT EPEC for the indicated times. Also shown is the total level of Cdc42 in the lysates ("total").

Figure 5. Factors determining Frabin recruitment to the pedestal.

(**A**) Fluorescence microscopy images of actin pedestals formed on WT HAP1 cells expressing dsRed-Frabin (red) and a PIP2 marker (the PH domain from phospholipase C δ1 fused to EGFP; green) by WT EPEC, Δ*espG* EPEC or Δ*tir* EPEC transformed with a plasmid encoding Tir^{Y474A} (blue). Bottom panels show pixel (fluorescence) intensity plots, measured along indicated lines in micrographs. (**B**) SDS/PAGE analysis and Coomassie Blue staining of proteins present on PC:PI or PC:PI:PIP2 (PIP2) bilayers anchored with the proteins indicated in the cartoons ($Arf6^{QL}$ alone or with co-anchored EspG), following incubation with increasing concentrations of purified, recombinant Frabin. Mobility of Frabin, EspG and Arf6 are indicated on the right-hand side of each panel (green triangle, brown square and red circle respectively). Asterisk indicates a minor contaminant in the recombinant EspG preparation that interacts with PC:PI bilayers and migrates slightly above the position of Frabin. (**C**) Fluorescence microscopy images of actin pedestals formed by WT EPEC (blue) on WT HAP1 cells transfected with dsRed-Frabin (red), PIP2 marker (green) and either $EspG^{\Delta A}$ or PH-$EspG^{\Delta A}$, as indicated. Bottom panels show pixel (fluorescence) intensity plots, measured along indicated lines in micrographs. (**D**) Model of Frabin's role in pedestal assembly. See discussion for full description.

Supplementary Figure Legends

Figure S1

(**A**) Quantification of the the level of Cdc42 isolated by GST-GBD beads ("active") from lysates prepared from either uninfected Hap1 cells, or those infected with WT *Salmonella,* WT EPEC or Δ*escN* EPEC, as indicated. Level is quantified from western blot images shown in Figure 1A. Each bar represents the average from 3 separate experiments, error bars represent ± SD. *** $p<0.001$, NS = not significant (one-way ANOVA followed by a post hoc Dunnett comparison) relative to control uninfected cells.

(**B**) Quantification of the level of Cdc42 isolated by GST-GBD beads ("active") from lysates prepared from either uninfected Hap1 cells, or those infected with WT EPEC*,* Δ*espG* EPEC or Δ*map* EPEC, as indicated. Level is quantified from western blot images shown in Figure 1E. Each bar represents the average from 3 separate experiments, error bars represent ± SD. *** $p<0.001$, NS = not significant (one-way ANOVA followed by a post hoc Dunnett comparison) relative to control uninfected cells.

(**C**) (i) Immunoblot of the level of Cdc42 isolated by GST-GBD beads ("active") from lysates prepared from either uninfected LoVo cells, or those infected with WT EPEC*,* Δ*espG* EPEC, Δ*map* EPEC or Δ*espG*Δ*map* EPEC, as indicated. Also shown is the total level of Cdc42 in the lysates ("total").

(ii) Quantification of the western blots shown in (ii). Each bar represents the average from 3 separate experiments, error bars represent ± SD. *** $p<0.001$, ** $p<0.01$, NS = not significant (one-way ANOVA followed by a post hoc Dunnett comparison) relative to control uninfected cells.

(**D**) (i) Immunoblot of the level of Cdc42 isolated by GST-GBD beads ("active") from lysates prepared from either uninfected HeLa cells, or those infected with WT EPEC*,* Δ*espG* EPEC, Δ*map* EPEC or Δ*espG*Δ*map* EPEC, as indicated. Also shown is the total level of Cdc42 in the lysates ("total").

(ii) Quantification of the western blots shown in (ii). Each bar represents the average from 3 separate experiments, error bars represent ± SD. *** $p<0.001$, ** $p<0.01$, NS = not significant (one-way ANOVA followed by a post hoc Dunnett comparison) relative to control uninfected cells.

(**E**) (i) Immunoblot of the level of Cdc42 isolated by GST-GBD beads ("active") from lysates prepared from either uninfected Caco-2 cells, or those infected with WT EPEC*,* Δ*espG* EPEC, Δ*map* EPEC or Δ*espG*Δ*map* EPEC, as indicated. Also shown is the total level of Cdc42 in the lysates ("total").

(ii) Quantification of the western blots shown in (ii). Each bar represents the average from 3 separate experiments, error bars represent ± SD. *** $p<0.001$, ** $p<0.01$, NS = not significant (one-way ANOVA followed by a post hoc Dunnett comparison) relative to control uninfected cells.

Figure S2

(**A**) Quantification of the level of Cdc42 isolated by GST-GBD beads ("active") from lysates prepared from Hap1 cells infected with the indicated EPEC strains. Level is quantified from western blot images shown in Figure 2A. Each bar represents the average from 3 separate experiments, error bars represent ± SD. *** $p<0.001$, NS = not significant (one-way ANOVA followed by a post hoc Dunnett comparison) relative to control uninfected cells.

(**B**) Quantification of the level of Cdc42 isolated by GST-GBD beads ("active") from lysates prepared from either uninfected WT Hap1 cells, or EPEC-infected WT HAP1, ΔPAK1 Hap1 or ΔPAK1 cells pre-treated with PAK inhibitor, as indicated. Level is quantified from western blot images shown in Figure 2B. Each bar represents the average from 3 separate experiments, error bars represent ± SD. *** $p<0.001$, (one-way ANOVA followed by a post hoc Dunnett comparison) relative to control uninfected cells.

Figure S3

(**A**) Quantification of the level of Cdc42 isolated by GST-GBD beads ("active") from lysates prepared from either uninfected WT Hap1, or EPEC-infected WT or ΔFrabin Hap1 cells. Level is quantified from western blot images shown in Figure 3A. Each bar represents the average from 3 separate experiments, error bars represent ± SD. *** $p<0.001$, * $p<0.1$ (one-way ANOVA followed by a post hoc Dunnett comparison) relative to control uninfected cells.

(**B**) Quantification of the level of active (phosphorylated on serine 144; PAK-P) PAK in uninfected WT Hap1 cells, and EPEC-infected WT or ΔFrabin cells, with and

without pretreatment with Rac inhibitor EHT 1864. Level is quantified from western blot images shown in Figure 3B, and normalised by the level of total PAK. Each bar represents the average from 3 separate experiments, error bars represent ± SD. *** p<0.001, * p<0.1 (one-way ANOVA followed by a post hoc Dunnett comparison) relative to control uninfected cells.

(**C**) Quantification of the attachment of EPEC to HeLa, LoVo or Caco-2 cells (as indicated) treated with Frabin siRNA, relative to untreated cells. Each bar represents the average of results from 3 separate experiments (100 to 200 cells for each replicate, 300-500 cells in total). Error bars indicate SD. **, $P < 0.01$ (by one-way analysis of variance [ANOVA] followed by a *post hoc* Dunnett comparison).

(**D**) Western blot showing the level of Frabin in cells treated with Frabin siRNA, as described in (D).

Figure S4

(**A**) Quantification of the level of Cdc42 isolated by GST-GBD beads (“active”) from lysates prepared from ΔFrabin HAP1 cells transfected with the indicated Frabin constructs and infected with WT EPEC. Level is quantified from western blot images shown in Figure 4B. Each bar represents the average from 3 separate experiments, error bars represent ± SD. *** p<0.001, ns = not significant (one-way ANOVA followed by a post hoc Dunnett comparison) relative to control uninfected cells.

(**B**) Quantification of the level of active (phosphorylated on serine 144; PAK-P) PAK in ΔFrabin HAP1 cells transfected with the indicated Frabin constructs and infected with WT EPEC. Level is quantified from western blot images shown in Figure 4C, and normalised by the level of total PAK. Each bar represents the average from 3 separate experiments, error bars represent ± SD. *** p<0.001, ns = not significant (one-way ANOVA followed by a post hoc Dunnett comparison) relative to control uninfected cells.

(**C**) Quantification of the level of Cdc42 isolated by GST-GBD beads (“active”) from lysates prepared from either untransfected (control) WT Hap1 cells, or those transfected with a plasmid expressing EspH (pEspH). Cells were either uninfected (-) or infected with WT EPEC for the indicated times. Level is quantified from western blot images shown in Figure 4F. Each bar represents the average from 3 separate experiments, error bars represent ± SD. *** p<0.001, ** $P < 0.01$, ns = not significant

(one-way ANOVA followed by a post hoc Dunnett comparison) relative to control uninfected cells.

A

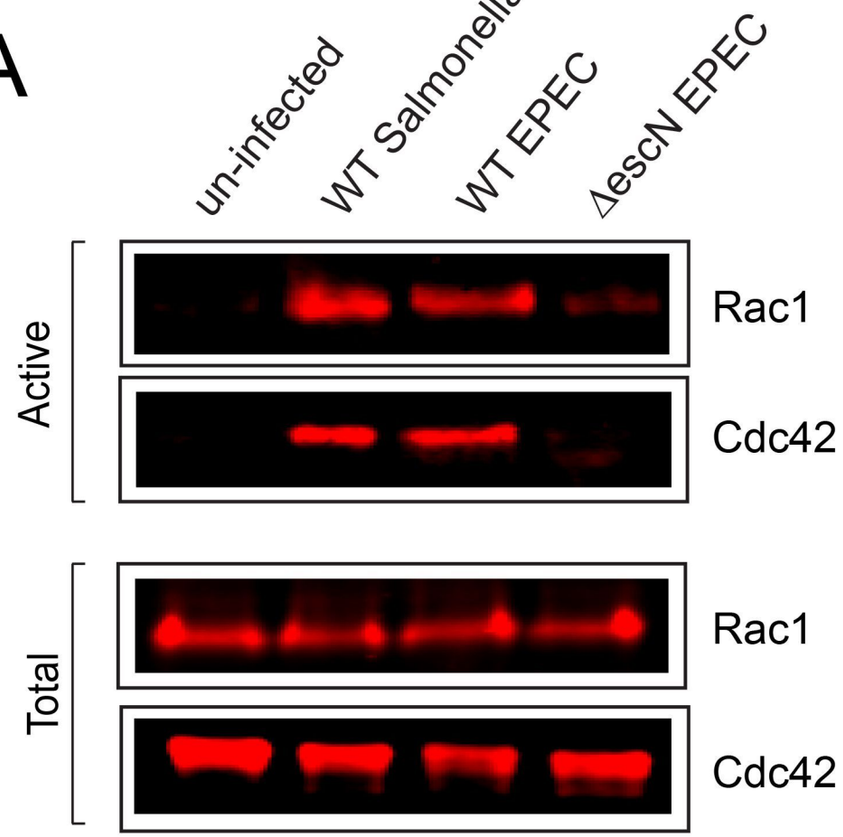
un-infected
WT Salmonella
WT EPEC
ΔescN EPEC
Active
Rac1
Cdc42
Total
Rac1
Cdc42

B

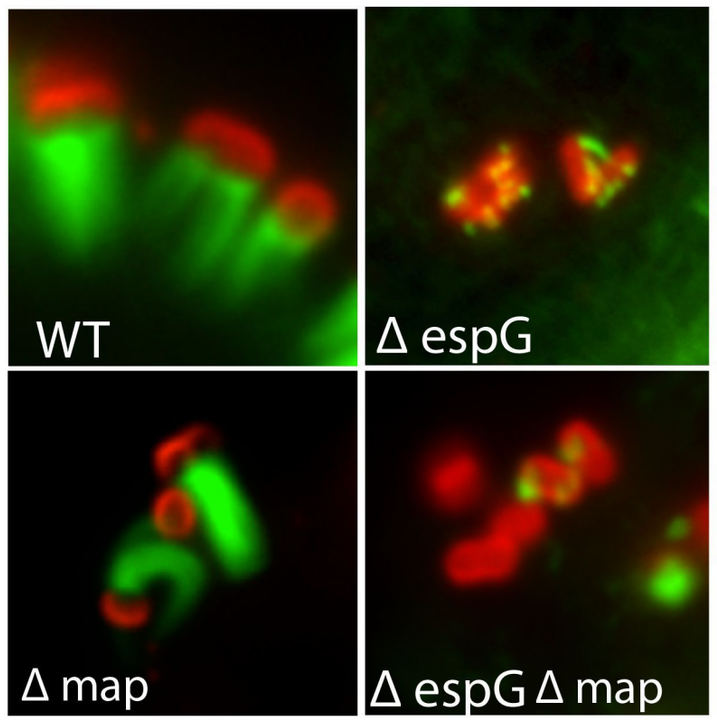
WT
Δ espG
Δ map
Δ espG Δ map

C

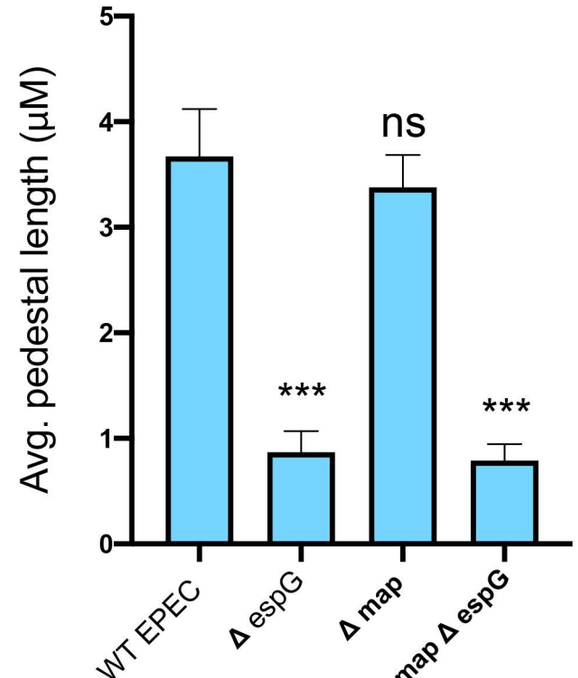
Avg. pedestal length (μM)
0
1
2
3
4
5
ns
***
***
WT EPEC
Δ espG
Δ map
Δ map Δ espG

D

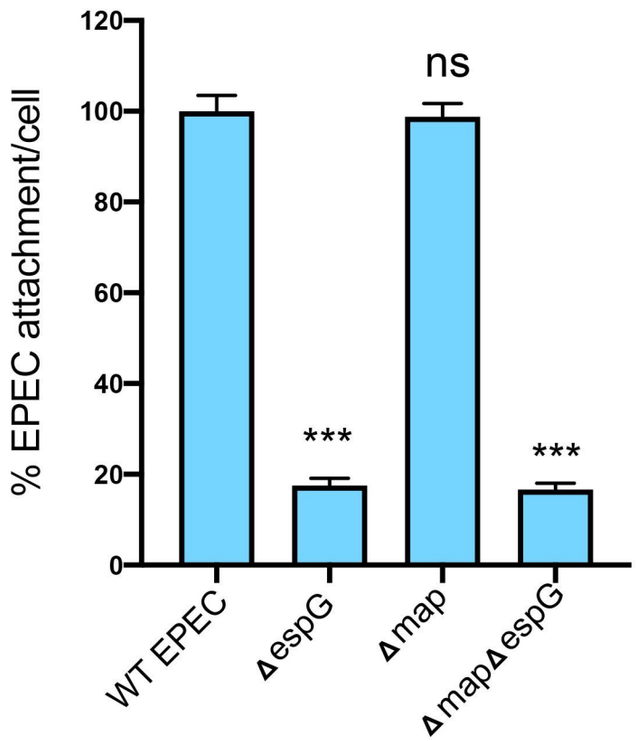
% EPEC attachment/cell
0
20
40
60
80
100
120
ns
***
***
WT EPEC
ΔespG
Δmap
ΔmapΔespG

E

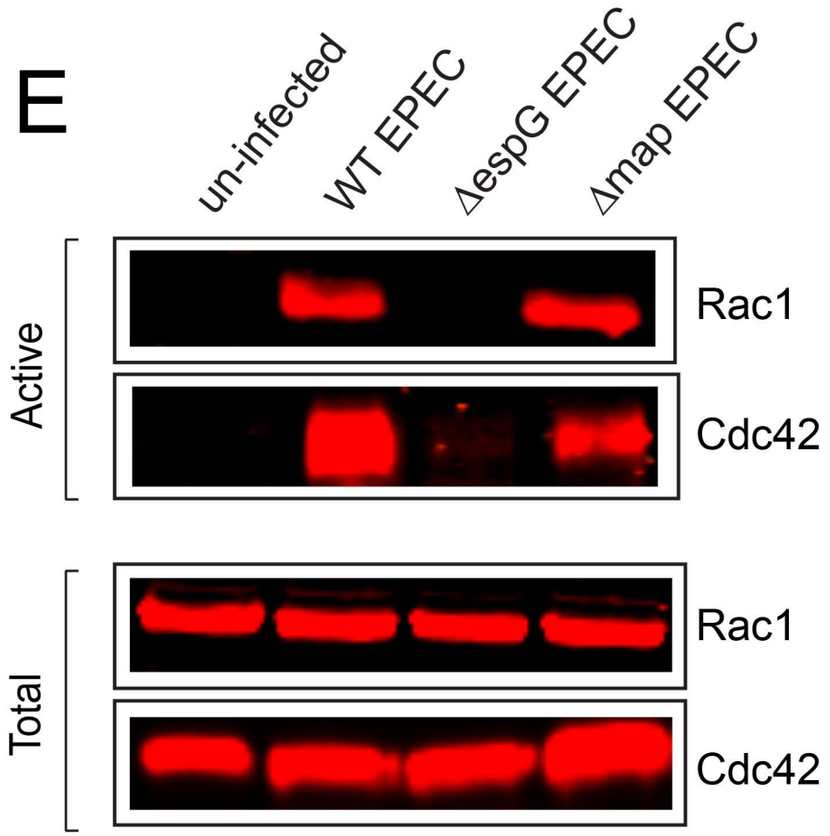
un-infected
WT EPEC
ΔespG EPEC
Δmap EPEC
Active
Rac1
Cdc42
Total
Rac1
Cdc42

A

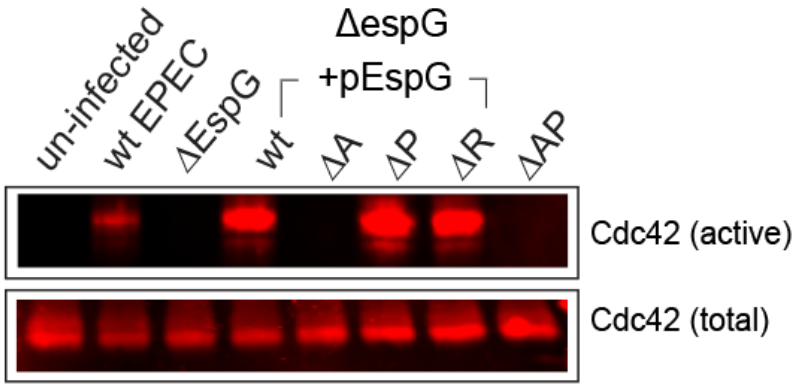

B

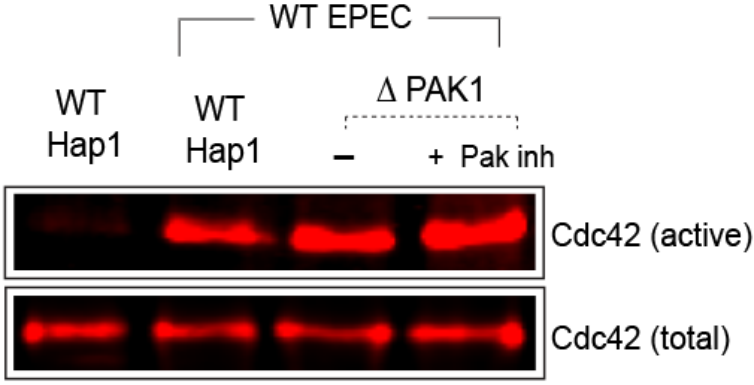

C

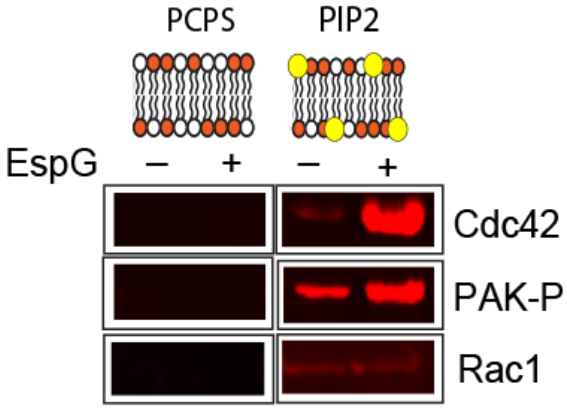

D

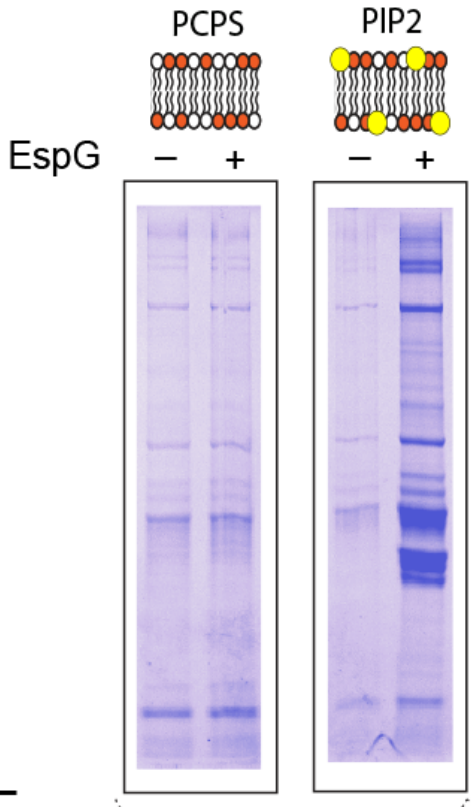

E

Prot_score	Protein	Predicted function
1893	Myosin-XVIIIa	Links Golgi membrane to the cytoskeleton
874	Frabin	Activates CDC42 & Rac1, deletion causes Charcot-Marie Tooth Disease
754	Formin-2	Actin-binding protein involved in actin cytoskeleton assembly
655	TIP47	Transports mannose 6-phosphate receptors from endosomes to trans-Golgi network
610	Septin 11	Filament forming cytoskeleton GTPase
557	Rho GTPase activating protein 32	GTPase Activating Protein (GAP) promoting GTP hydrolysis on RHOA, CDC42 and RAC1
495	Heat shock protein 70	Acts as Chaperone, activated upon stress

F

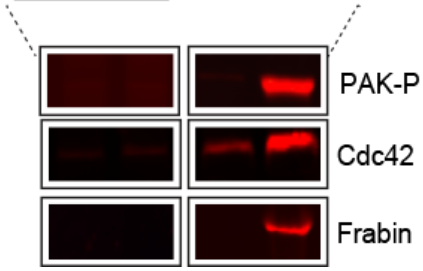

A

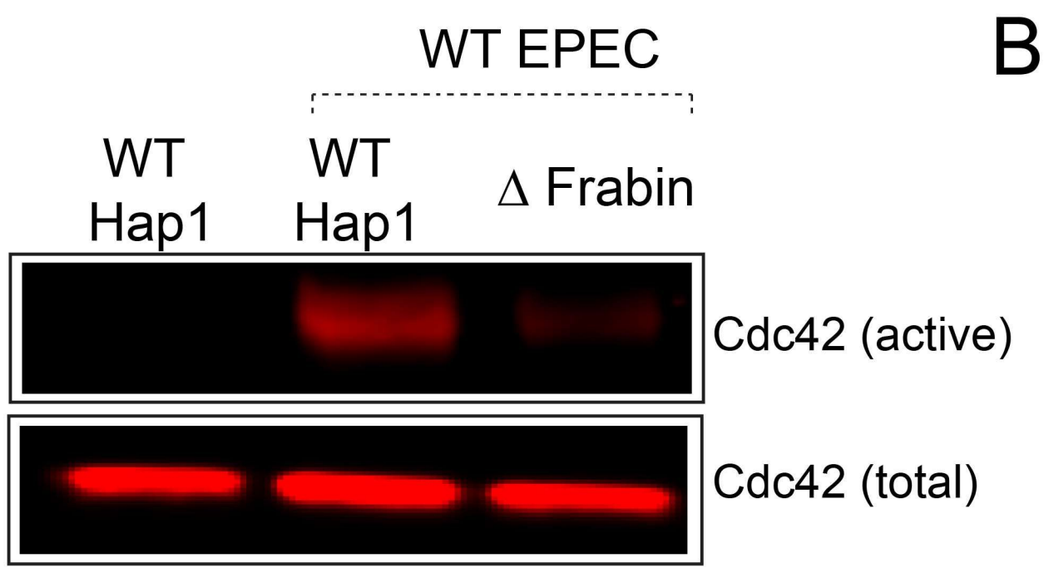
WT EPEC
WT Hap1
WT Hap1
Δ Frabin
Cdc42 (active)
Cdc42 (total)

B

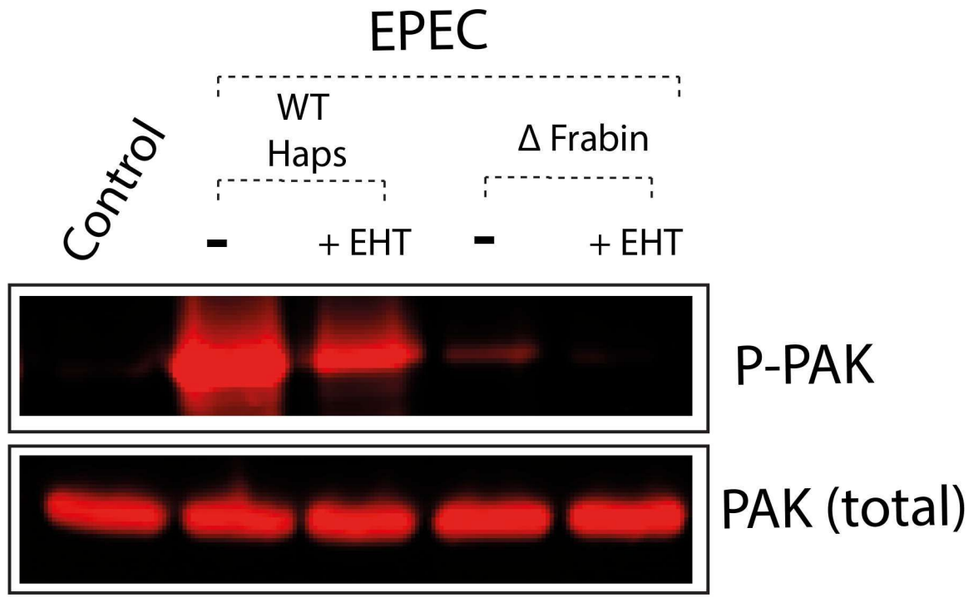
EPEC
Control
WT Haps
Δ Frabin
-
+ EHT
-
+ EHT
P-PAK
PAK (total)

C

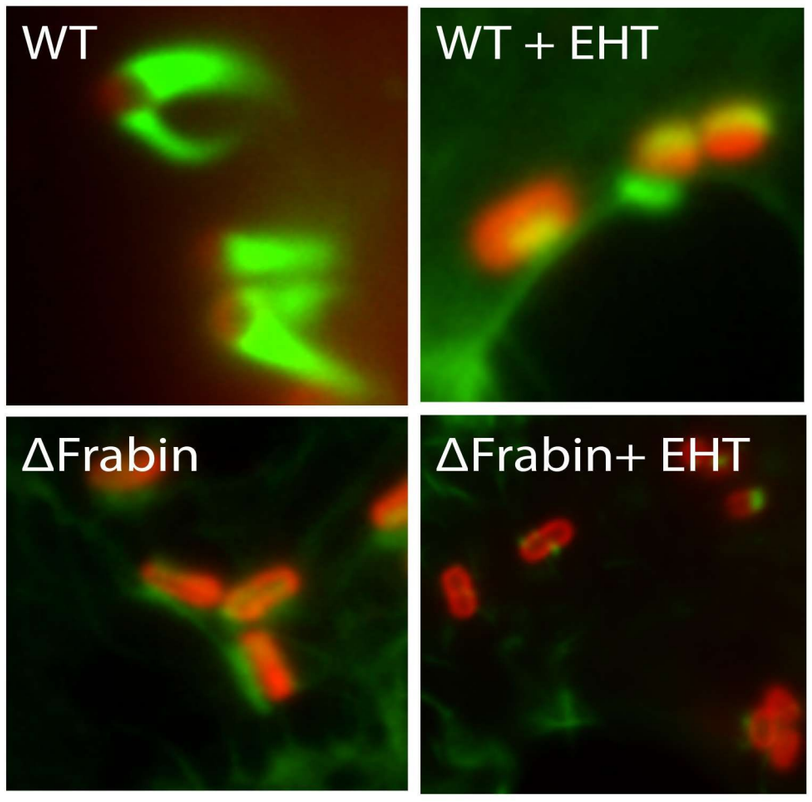
WT
WT + EHT
ΔFrabin
ΔFrabin+ EHT

D

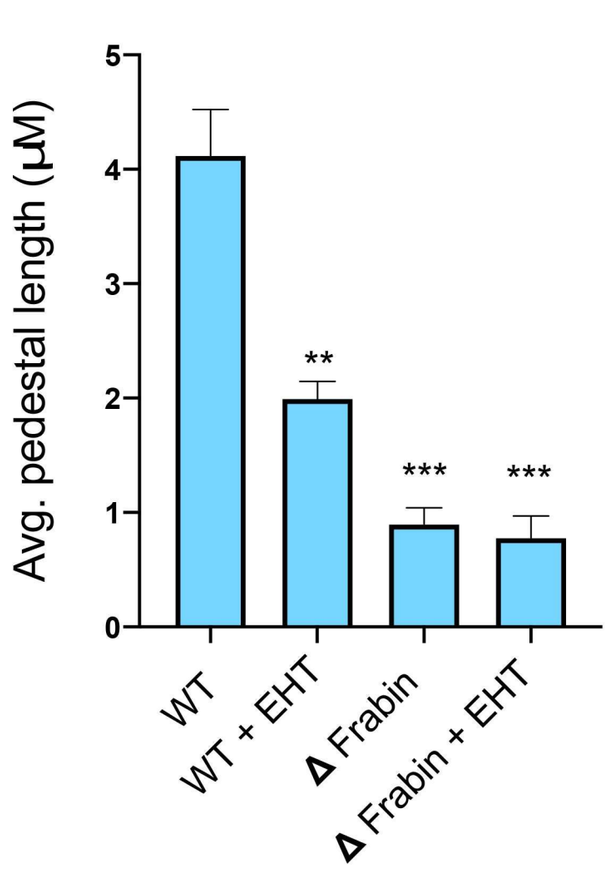
Avg. pedestal length (μM)
0
1
2
3
4
5
**
***
***
WT
WT + EHT
Δ Frabin
Δ Frabin + EHT

E

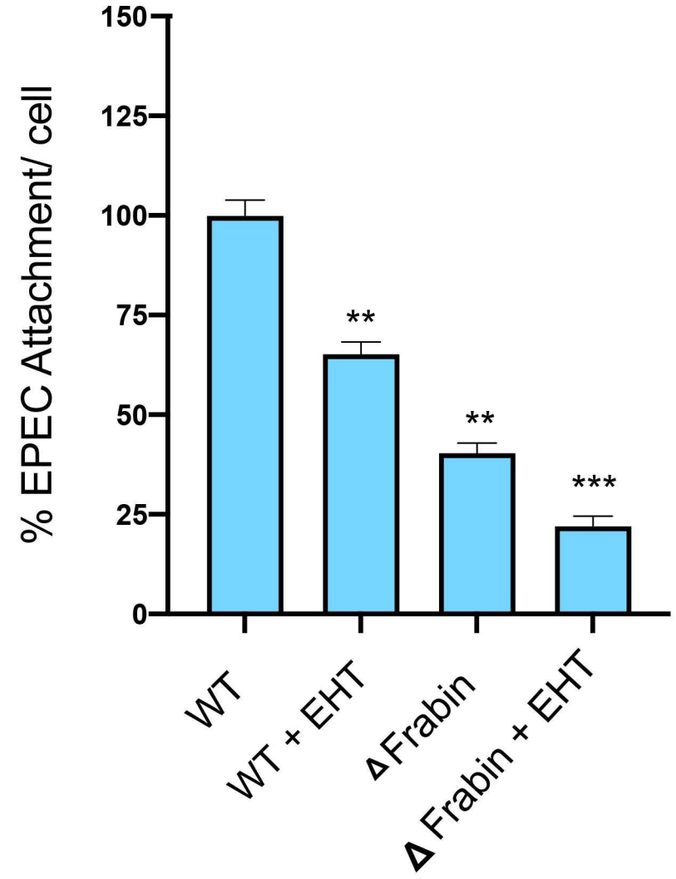
% EPEC Attachment/ cell
0
25
50
75
100
125
150
**
**
***
WT
WT + EHT
Δ Frabin
Δ Frabin + EHT

A

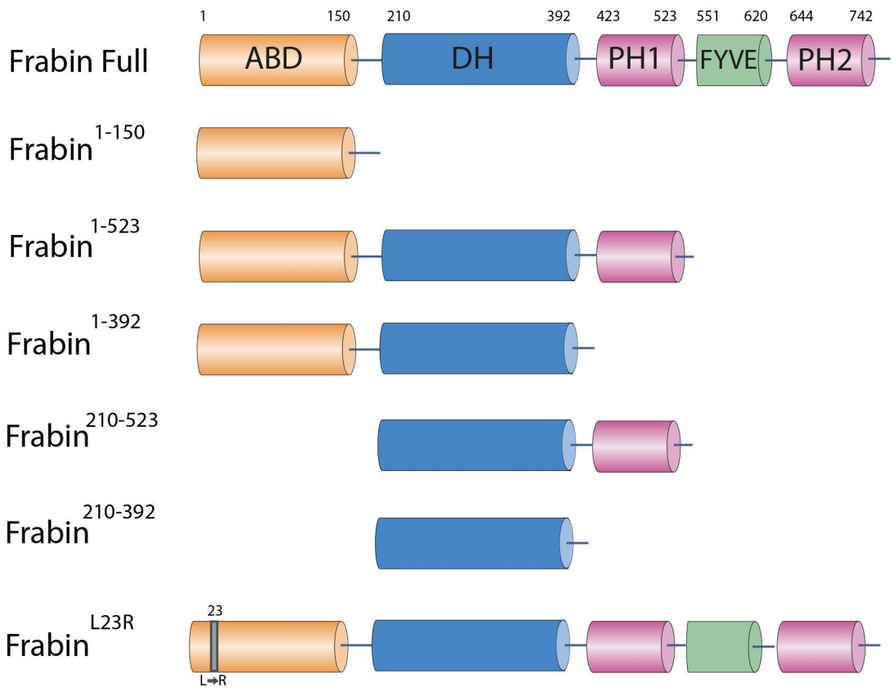
1
150
210
392
423
523
551
620
644
742
Frabin Full
ABD
DH
PH1
FYVE
PH2
Frabin 1-150
Frabin 1-523
Frabin 1-392
Frabin 210-523
Frabin 210-392
Frabin L23R
23
L→R

B

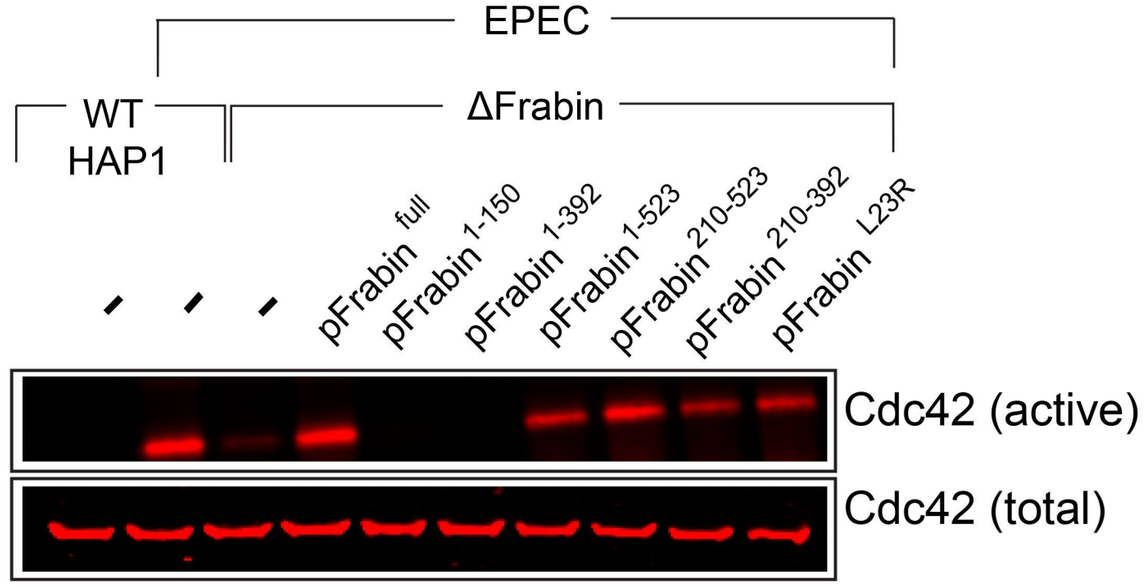
EPEC
WT HAP1
ΔFrabin
pFrabin full
pFrabin 1-150
pFrabin 1-392
pFrabin 1-523
pFrabin 210-523
pFrabin 210-392
pFrabin L23R
Cdc42 (active)
Cdc42 (total)

C

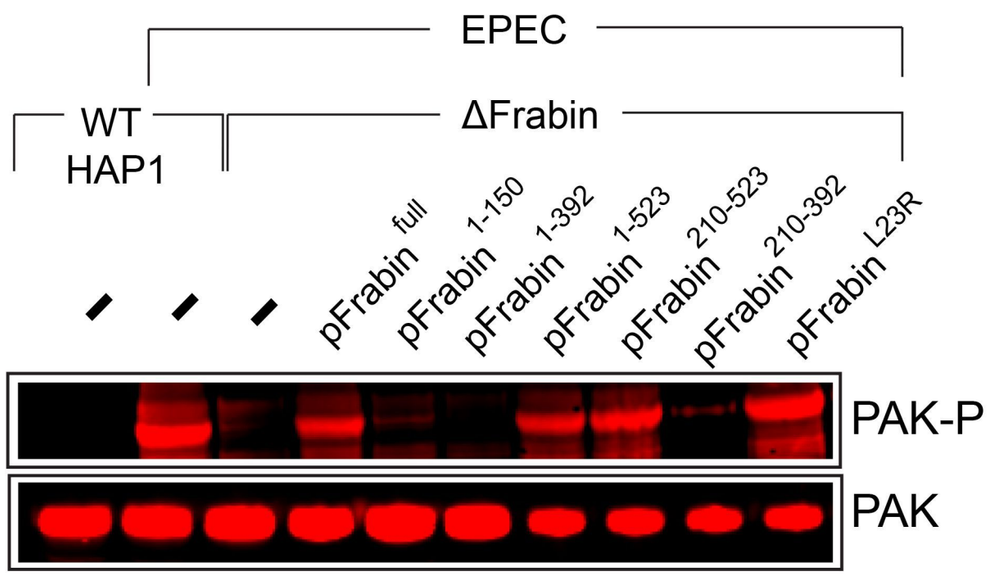
EPEC
WT HAP1
ΔFrabin
pFrabin full
pFrabin 1-150
pFrabin 1-392
pFrabin 1-523
pFrabin 210-523
pFrabin 210-392
pFrabin L23R
PAK-P
PAK

D

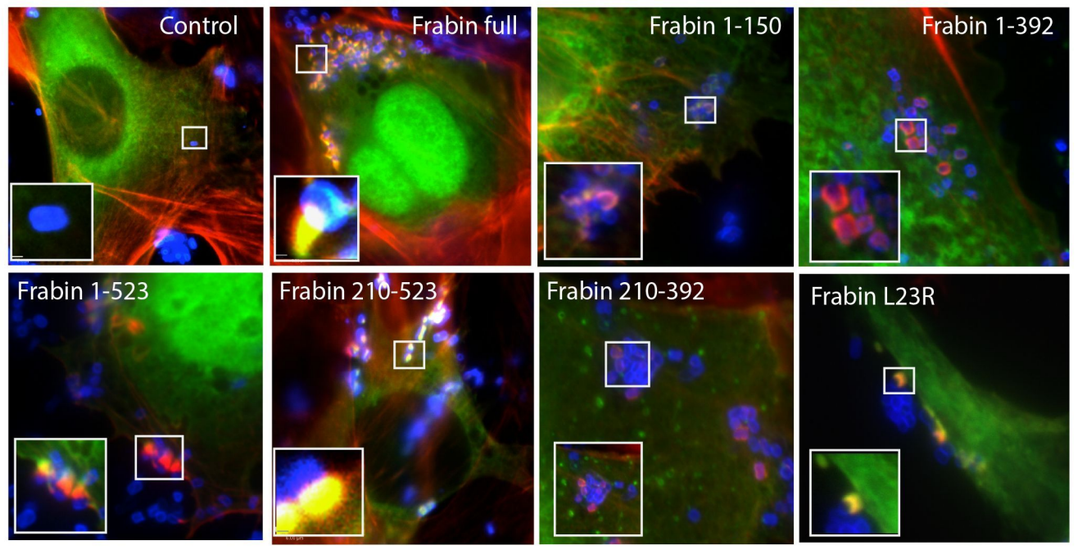
Control
Frabin full
Frabin 1-150
Frabin 1-392
Frabin 1-523
Frabin 210-523
Frabin 210-392
Frabin L23R

E

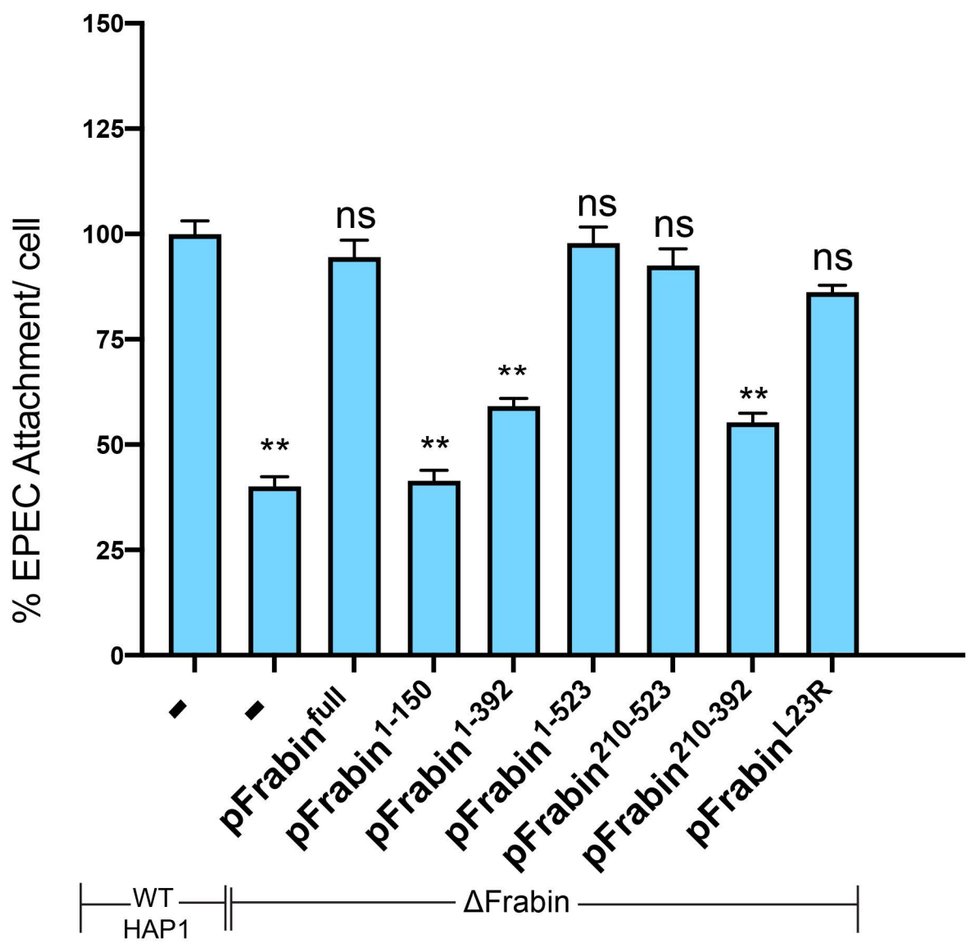
% EPEC Attachment/ cell
150
125
100
75
50
25
0
ns
**
pFrabin full
pFrabin 1-150
pFrabin 1-392
pFrabin 1-523
pFrabin 210-523
pFrabin 210-392
pFrabin L23R
WT HAP1
ΔFrabin

F

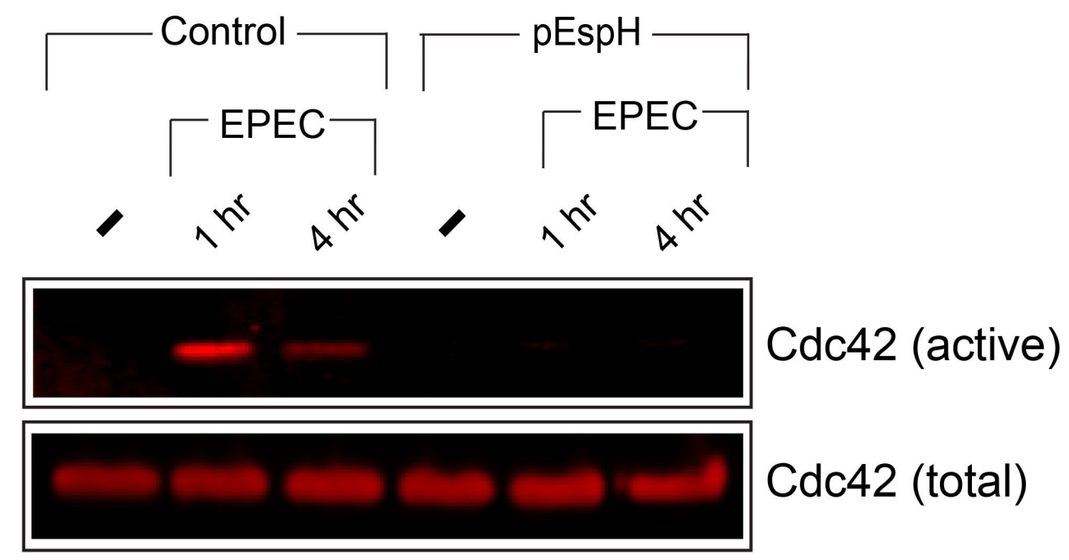
Control
pEspH
EPEC
EPEC
1 hr
4 hr
1 hr
4 hr
Cdc42 (active)
Cdc42 (total)

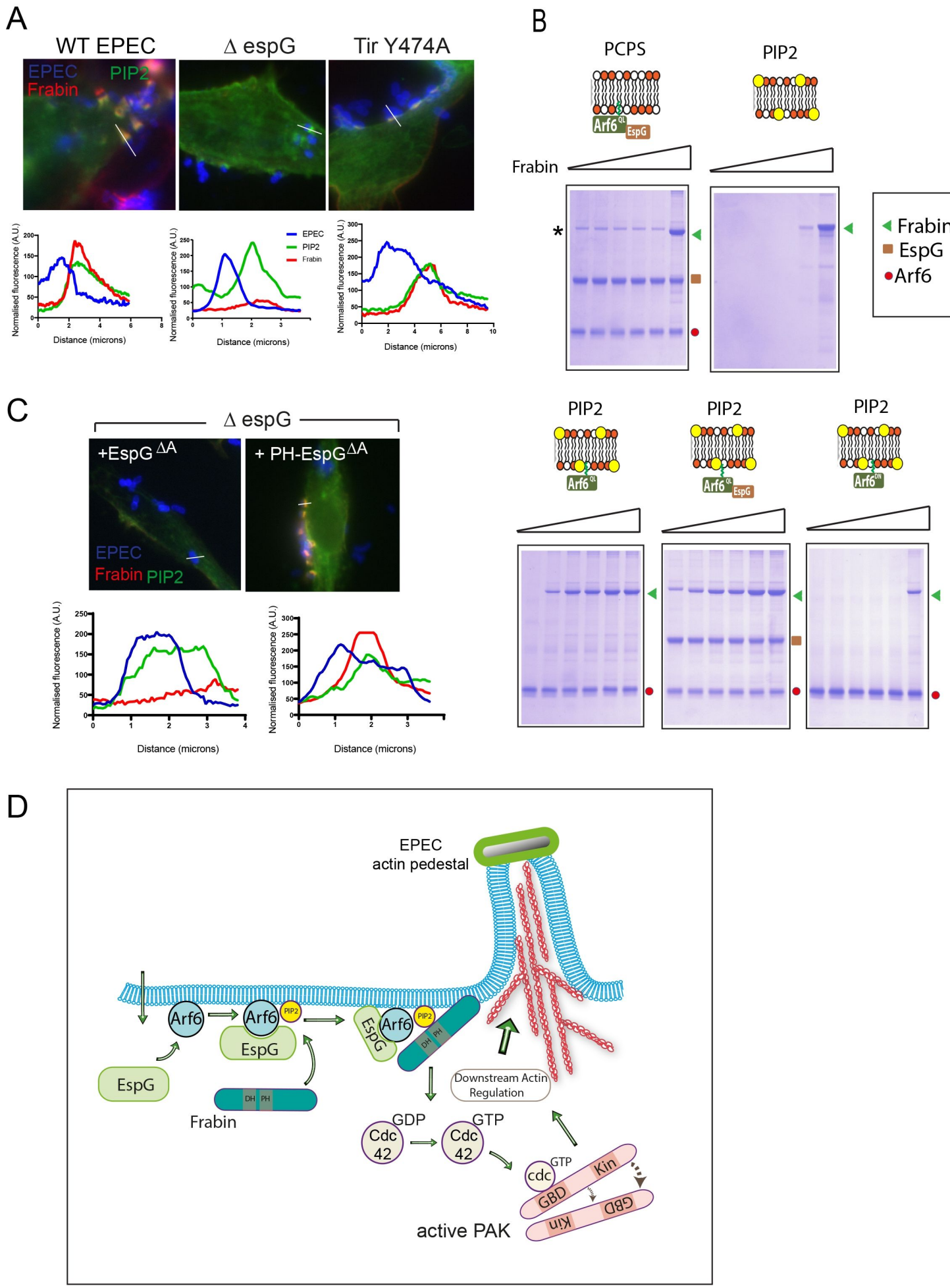
A
WT EPEC
Δ espG
Tir Y474A
EPEC
Frabin
PIP2
Normalised fluorescence (A.U.)
Distance (microns)
EPEC
PIP2
Frabin
B
PCPS
PIP2
Arf6 QL
EspG
Frabin
*
Frabin
EspG
Arf6
C
Δ espG
+EspG ΔA
+ PH-EspG ΔA
EPEC
Frabin
PIP2
Normalised fluorescence (A.U.)
Distance (microns)
PIP2
PIP2
PIP2
Arf6 QL
Arf6 QL
EspG
Arf6 DN
D
EPEC
actin pedestal
Arf6
PIP2
EspG
DH
PH
Frabin
Downstream Actin
Regulation
GDP
GTP
Cdc
42
cdc
GTP
Kin
GBD
active PAK